acoustics

MDPI

Article

Investigations into the Approaches of Computational Fluid Dynamics for Flow-Excited Resonator Helmholtz Modeling within Verification on a Laboratory Benchmark

Daniil Sergeev [1,*], Irina V'yushkina [1], Vladimir Eremeev [1], Andrei Stulenkov [1] and Kirill Pyalov [2]

[1] Federal Research Center A.V. Gaponov-Grekhov Institute of Applied Physics of the Russian Academy of Sciences (IAP RAS), 46 Ul'yanov Street, Nizhny Novgorod 603950, Russia; volkova@ipfran.ru (I.V.); eremeev.vladimir.o@ipfran.ru (V.E.); stulenkov@ipfran.ru (A.S.)

[2] Joint-Stock Company "Central Design Bureau for Marine Engineering "Rubin" (CDB ME "Rubin") 90, Marata Str., Saint Petersburg 191119, Russia; kir-pyalov@yandex.ru or neptun@ckb-rubin.ru

* Correspondence: daniil@ipfran.ru

Abstract: This paper presents the results of a study of self-sustained processes excited in a Helmholtz resonator after a flow over its orifice. A comparative analysis of various approaches to the numerical modeling of this problem was carried out, taking into account both the requirements for achieving the required accuracy and taking into account the resource greediness of calculations, the results of which were verified by comparison with data obtained during a special experiment. The configuration with a spherical resonator with a natural frequency of 260 Hz and an orifice diameter (about 5 cm) in an air flow with a speed of 6 to 14 m/s was considered. A comparison of the calculation results with data obtained in experiments carried out in the wind tunnel demonstrated that the accuracy of calculations of the characteristics of the self-sustained mode using the simplest URANS class model tends to the accuracy of calculations within the large eddy simulation approach formulated in the WMLES model. At the same time, when using WMLES, it is possible to better reproduce the background level of pulsations. From the point of view of resource greediness, expressed in the number of core hours spent obtaining a solution, both models of the turbulence turned out to be almost equivalent when using the same grid models.

Keywords: Helmholtz resonator; self-sustained oscillations; computational fluid mechanics; URANS; scale resolving simulation; resource greediness

check for updates

Citation: Sergeev, D.; V'yushkina, I.; Eremeev, V.; Stulenkov, A.; Pyalov, K. Investigations into the Approaches of Computational Fluid Dynamics for Flow-Excited Resonator Helmholtz Modeling within Verification on a Laboratory Benchmark. *Acoustics* **2024**, *6*, 18–34. https://doi.org/10.3390/acoustics6010002

Academic Editors: Li Cheng and Nikolay Kanev

Received: 7 November 2023
Revised: 28 November 2023
Accepted: 6 December 2023
Published: 22 December 2023

Copyright: © 2023 by the authors. Licensee MDPI, Basel, Switzerland. This article is an open access article distributed under the terms and conditions of the Creative Commons Attribution (CC BY) license (https://creativecommons.org/licenses/by/4.0/).

1. Introduction

A 'Helmholtz resonator' is a device in which a volume of compressible fluid is enclosed by rigid boundaries with a single, small orifice [1]. The resonator is easily modelled by a second-order mass-spring system analogy, where the fluid in the region of the orifice acts as the effective mass, and the compressibility of the fluid in the volume acts as the stiffness. Acoustic radiation and viscous effects both lead to effective damping. The resonator's natural frequency can be simply estimated as $f_{\text{res}} = c/2\pi\sqrt{S/Vl}$, where S is the area of the orifice; l is the effective neck thickness; V is the volume of the resonator; and c is the speed of sound. Near this frequency, a small pressure disturbance can produce a large-magnitude velocity fluctuation at the orifice and thus a large pressure fluctuation within the resonator.

Such a resonance system can be excited acoustically at frequencies close to the resonance one. This feature is used for noise reduction applications. In this case, systems of one or several relatively large resonators (dimensions comparable to the typical scales of the flow) are used, for example, as installed on benchmarks [2], when actually operating technical devices such as engines and fans [3], and in covering materials with special perforations, in which some cells are like microresonators [4]. Also, special metamaterials are being developed that use combinations of cavities (resonators) with different parameters

for damping/selecting noise (see, for example, [5]). But more interesting from a physical point of view is the so-called flow-excited resonator Helmholtz case. A very well-known example of this phenomenon is the resonance that occurs when blowing over the orifice of a glass bottle. The same physical process is present when an automobile is traveling with a single window lowered. This is often termed 'window buffeting' and results in an uncomfortable level of cabin pressure fluctuation. The physics of this process are that the shear layer is linearly unstable to disturbances for discrete numbers of the nondimensional Strouhal number fL/U (the parameter related to the generation of sound by unsteady flows), where f is the oscillation frequency and L is the size of the orifice along the flow (for example, [6,7]). In this case, the excitation of resonance oscillations generated by the flow occurs when one of the frequencies of hydrodynamic instability is close to the natural frequency of the resonator f_{res}. In other words, the pressure fluctuations in the resonator are the maximum at the specific velocity at which the frequency of the most unstable shear layer mode is equal to the frequency of the resonator. In most applications, notably for the glass bottle and automobile window, the velocity at which the fluctuations are the maximum will be at a relatively low Mach number, say $M < 0.1$; however, compressibility cannot be neglected in these cases.

Early works on the study of the flow of the Helmholtz resonator mainly concerned the description of the acoustics of resonators of different sizes and configurations with different conditions of the exciting flow [8,9] without a detailed study of the mechanisms of occurrence of self-sustained oscillations. In [10], detailed measurements of both the pressure in the resonator and the flow field near the orifice were carried out for the first time. These data were subsequently used to verify calculations in a number of studies. Thus, on their basis, in [11], a flow analysis was performed based on the use momentum and energy budget in a linear approximation. The effect of orifice shape on fluctuations inside the resonator was studied in investigations [12–15]. For an orifice with a deep neck, a model based on the so-called feedback loops was proposed in [16]. The hydrodynamic forcing was considered a "forward gain function" and the acoustics in the resonator were considered a "backward gain function". The pressure amplitude inside the resonator was calculated by equating the amplitude and phase of the two gain functions. This method was further developed in [17], in which an analytical description of the direct gain function was proposed. Using a certain dimensionless adjusting parameter β, the theory was for the first time able to describe accurately the dependence of the pressure amplitude in the resonator on the free-stream velocity. Later, a modified version of this method by modeling the direct gain function in the point vortex approximation was developed in [18]. This work demonstrates that it was possible to introduce an adjusting parameter α that allowed the theory to accurately predict pressure in a resonator over a wide range of free-stream conditions.

The role of panoramic methods based on visualization in studying the characteristics of acoustic and hydrodynamic fields in the Helmholtz resonator problem should be mentioned, additionally. Thus, in [19], studies of the parameters of resonance modes inside a resonator excited in an impedance pipe using fog visualization in a laser sheet was combined with the measurements of pneuma gauges and microphones. The fog visualization allowed a clear demonstration for the first time that resonance is caused by the disruption of a single discrete vortex from the edge of the orifice, which moves along it during one cycle of oscillations (the first mode) in studies of the flow-excited Helmholtz resonator ([10]). A significant breakthrough was made in [20], using well-established methods for measuring flow velocity fields' Particle Image Velocimetry (PIV) (for a description, see [21]). Here, the authors also used an analysis based on the use of the momentum equation to understand the relationship between the shear hydrodynamic instability of the boundary layer and the pressure instability in the resonator. They found that unsteady circulation (i.e., the integral area of the vortex over the orifice region) acted as a quantitative characteristic of the forcing on the resonator. The calculations of the pressure in the resonator carried out in [20], based on the results of measurements of velocity fields, found good agreement within

3 dB with the results of measurements by microphones in a wide range of flow velocities. Thus, data on the flow velocity field near the orifice make it possible not only to obtain an estimation of the spatiotemporal structure of the hydrodynamic instability mode that initiates self-sustained oscillations, but also to obtain a quantitative estimate for pressure pulsations. Note that, unlike point measurements of sound pressure, PIV measurements of the velocity fields are very complex, especially on real technical systems. In this case, data on the flow velocity field can be obtained using computational fluid dynamics (CFD) numerical simulation, which is discussed below.

It should be noted that most of the laboratory measurements and theoretical studies use model conditions to evaluate the basic physical processes occurring in such systems. Thus, experiments with the free-flow-induced self-sustained oscillations are carried out in wind tunnels, where it is possible to control, vary and measure the flow parameters, or resonators are excited in special impedance pipes by controlled sound sources. In this case, resonators of the simplest configuration are used (rectangular, cylindrical, less often spherical, etc.), for which their own resonance modes can be measured/calculated well. Theoretical models developed using empirical data can describe such simplified problems well, but can often be used only for an approximate (qualitative) description of processes occurring in complex technical systems; for example, internal aeroacoustics of different vehicles (primarily car interiors), noise damping systems in various types of propulsion systems, climate control equipment, etc. Rapidly developing CFD methods can provide significant assistance here well as in many other studies of aero-hydrodynamic systems. However, the peculiarities of using CFD should be taken into account when the compressibility of the medium cannot be neglected, playing a fundamental role in the systems considered in this work.

Taking into account that compressibility leads to the need to solve an additional equation connecting pressure and density changes, this inevitably leads to an increase in resource costs compared to the incompressible formulation. In addition, it should be noted that acoustic disturbances in amplitude are of a much lower order than disturbances associated with the formation of vortex structures, which is why it is often necessary to use data storage in a 64-bit system, instead of in a 32-bit system, which is sufficient for incompressible productions. This affects the required RAM doubling, which for large problems (in terms of the number of grid model elements) is no less problematic than the calculation speed.

Another complicating factor is concerned with adjusting the discretization time step in calculations. A Courant–Friedrichs–Lewy criterion, which characterizes the disturbance spatial transfer in space over a fixed time interval, is used for choosing this important parameter in CFD procedures:

$$\frac{u_x \Delta t}{\Delta x} + \frac{u_y \Delta t}{\Delta y} + \frac{u_z \Delta t}{\Delta z} < 1, \tag{1}$$

where u_x, u_y, u_z are components of velocity transfer, Δx, Δy, Δz are the spatial discretization scale, and Δt is the discretization time step. Criterion (1) means that the disturbance should not be advected more than the spatial discretization scale per time step. Here, again, we should recall the fundamental need to take into account compressibility for the occurrence of self-sustained oscillations in the systems under consideration in this work, despite the fact that the velocities of the exciting flow above the hole satisfy the condition $M \ll 1$. Taking into account condition (1), for such problems the time step must be reduced by $n = c/U$ times, with a corresponding increase in calculation time by n times compared to problems of incompressible flows.

Seeking a compromise between the quality of the results obtained (usually verified with measurement data), greediness resources and calculation time is a usual feature when using CFD methods to study any hydrodynamic system, and especially when solving applied problems for various kinds of complex technical devices. The need to take into account the compressibility of the medium, which is the main factor in systems such as

the Helmholtz resonator considered in this work, leads to higher resource/time requirements compared to an incompressible medium. In this regard, attempts to use simplified approaches to describe Helmholtz resonators excited by flows have been made from the very beginning of the use of CFD methods. For example, in [19], a certain intermediate approximation was used between the conditions of a compressible and incompressible medium for the Navier–Stokes equations, and in [20] a numerical procedure based on the kinetic equation, combined with the RNG turbulence model, is applied. In this case, it was possible to obtain good qualitative agreement; however, the calculated amplitudes of pressure pulsations could be lower (up to 20 dB, see [19]), and in [20] a special coefficient was even introduced to reduce the free flow velocity by 15/22 times compared to parameters of the experimental studies in [10] to demonstrate agreement between the calculated pressure values in the resonator and the experimental data. This was explained by the difficulties of adequately reproducing the velocity distribution in the boundary layer, the thickness of which affects the effective velocity of the shear layer. On the other hand, when carrying out calculations without any simplifications for modeling specific structures, resource greediness increases greatly. For example, in work [22], to calculate the buffering effects from a window inside a simplified model of a car like the Purdue cavity model with a scale of about 1:5 of the real size, it took 7 days of calculations for an implementation lasting only 0.25 s on a grid of 16 million nodes to achieve an accurate determination of pressure pulsations on the main modes of at least 10 dB (in comparison with a verification experiment in a wind tunnel).

It should be mentioned that no special research devoted to the choice of correct and optimal calculation parameters to obtain results with the required accuracy when solving problems of Helmholtz resonator excitation by a free flow has been carried out to solve this urgent problem. This work is intended to at least partially fill this gap.

The article has the following structure. The first part describes a special laboratory experiment performed in the wind tunnel of the Institute of Applied Physics RAS, the results of which were used to verify numerical model. The second part is devoted to a description of calculation procedures, including the turbulence models used, the computational grids, and a comparison of the results obtained with the experiments performed. At the end, there are the main conclusions.

2. Description of Experiment and Obtained Results

2.1. Scheme of Experiment and Carrying Out Measurements

A spherical resonator, shown in Figure 1, with the following characteristics—outer diameter: 170 mm, inner diameter: 150 mm, inside volume: 1.8 L, orifice diameter: 48 mm—was used in experiments. The resonator was made of plastic using 3D printing.

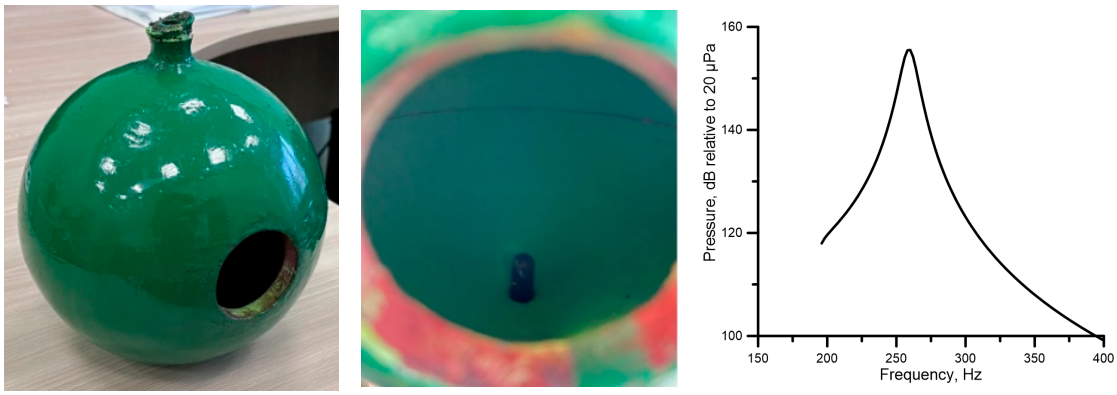

(**a**) (**b**) (**c**)

Figure 1. The resonator used in investigations: (**a**) common view, (**b**) microphone gauge installed inside resonator, (**c**) frequency response characteristic.

The frequency response characteristic of this object was obtained numerically using original software SATES 2.0 [23] (for details, see Section 3, below).

The experiments were carried out in the wind tunnel of the Institute of Applied Physics RAS (IAP RAS). The general scheme of the experiment was as follows: the resonator was placed in the working section of the wind tunnel with a cross-section of 300 × 300 mm and a length of 1170 mm (the layout is shown in Figure 2). The resonator was fixed on a vertical pipe, through which a microphone was inserted into the internal cavity of the resonator. Recordings were performed at a sampling rate of 5 kHz for 1 min. The smooth adjustment of the inlet airflow speed in the range of 0. . .14 m/s is allowed.

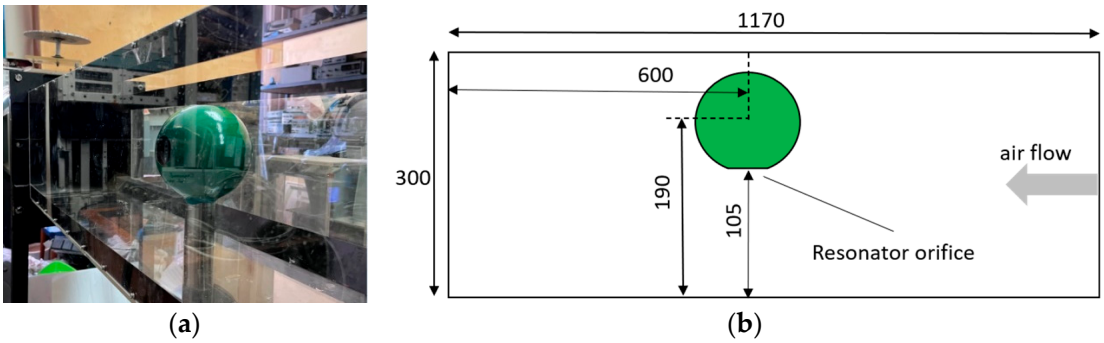

Figure 2. (**a**) Resonator installed in the working section of the wind tunnel of IAP RAS; (**b**) scheme of the location of the resonator inside the working section of the wind tunnel: top view, dimensions are given in mm.

The resonator in the working section was installed in the following way: the plane of the orifice of the resonator was vertically oriented, and the center of the orifice was at the height of the middle of the section. In this case, the resonator was close to one of the walls so that the plane of the orifice was close to the centerline of the section (at a distance of 105 mm from the side wall; see Figure 2b). The height of the center of the orifice relative to the bottom of the section was 170 mm.

The inlet airflow speed was controlled during the measurements by a calibrated hotfilm gauge E+E75 with low time resolution (frequency 5 Hz). Before each recording, this gauge was inserted into the flow through a special orifice to control the speed, and then removed, and the orifice was closed with a special plug to avoid parasitic disturbances.

Measurements of the air flow velocity were carried out directly in the area of the orifice, i.e., in the flow exciting the Helmholtz resonator, and were carried out simultaneously with measurements of sound pressure pulsations inside the resonator. Data were obtained using a Dantec two-component miniature hot-wire anemometer. The gauge was positioned vertically (fixed on the top cover), and the sensitive element on the end of the probe was located in the center of the orifice, at a distance of 5 mm or more from the plane of the orifice (see Figure 3) in these measurements. The gauge made it possible to obtain two velocity components in the horizontal plane perpendicular to the plane of the orifice with frequency 5 kHz. Recordings were performed for 1 min.

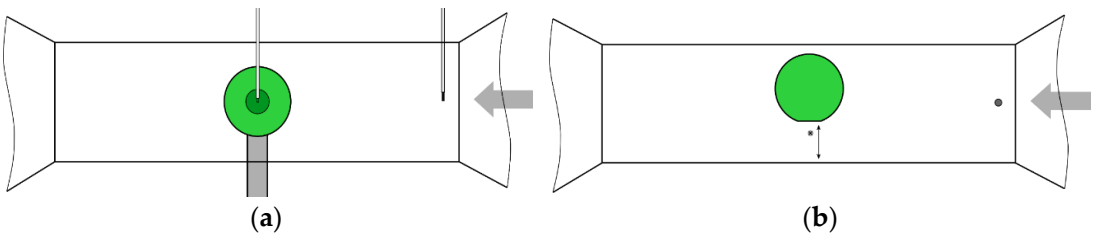

Figure 3. Scheme of measurements of air flow with hot film in the inlet and hot wire close to the resonator orifice anemometers relative to a resonator in a wind tunnel: (**a**) side view, (**b**) top view.

Measurements of sound pressure characteristics were carried out for a speed range from 4 to 14 m/s with a step of 0.5 m/s (for a total of twenty-one air flow speed values). Measurements of air flow velocity were carried out at five speeds: 8, 10, 12, and 14 m/s (for which numerical modeling was then performed) simultaneously with sound measurements.

2.2. Analysis of the Measurements Results

The simultaneous measurements of pulsations of pressure and flow velocity made it possible to compare the corresponding spectra (see Figure 4).

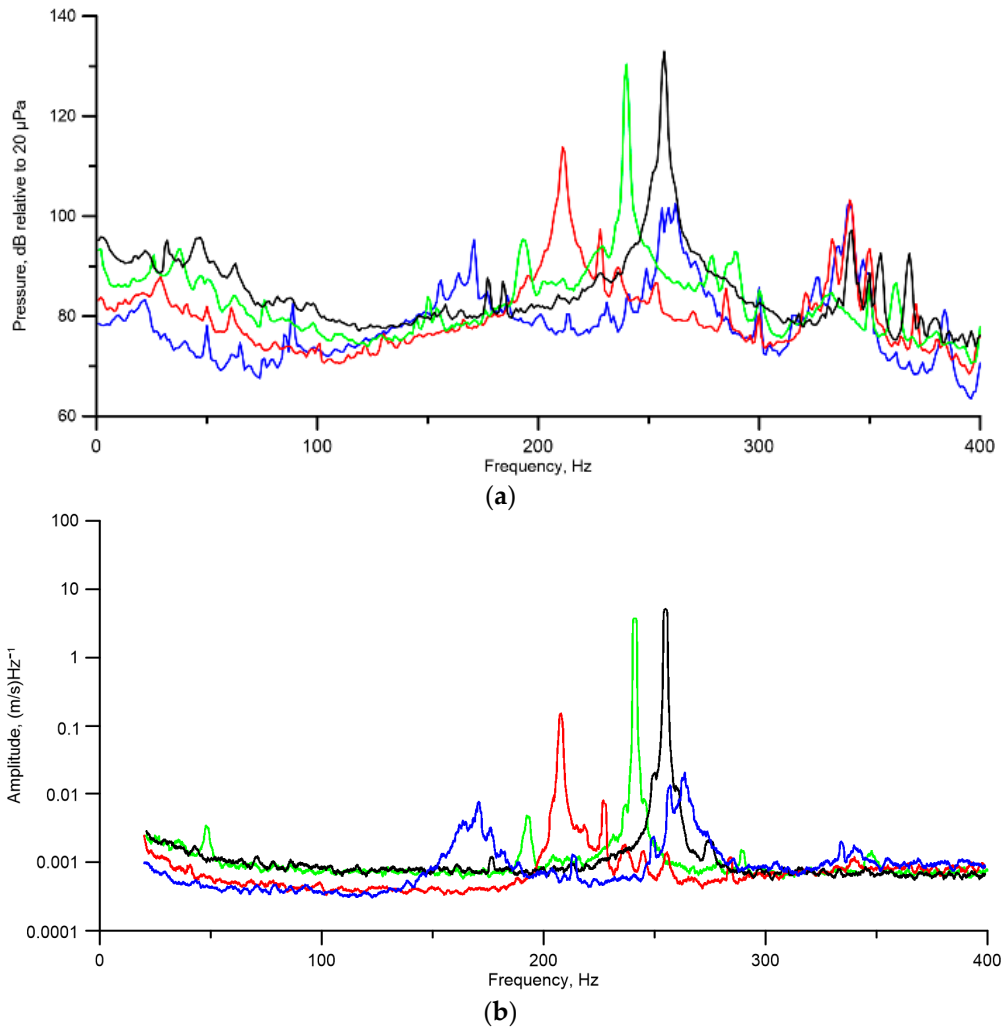

Figure 4. Frequency spectra in the range up to 400 Hz for different inlet airflow speeds: (**a**) pressure power pulsations inside the resonator; (**b**) flow velocity module pulsations at a distance of 5 mm above the orifice. Line color: blue—8 m/s, red—10 m/s, green—12 m/s, black—14 m/s.

The spectra clearly showed resonance-type narrow peaks in the range from 170 Hz to approximately 260 Hz. The spectra coincided well with each other. It should be noted that not only the frequencies corresponding to the peaks coincided, but also the peculiarities in the shapes of the spectra. Thus, the system implemented self-sustained oscillations due to the interaction of the mode of hydrodynamic instability of the flow above the orifice and acoustic modes of the resonator.

Analyzing the spectra, one can see that there was a pronounced narrow peak, the frequency and amplitude of which decreased as the air flow speed decreased from 14 to 10 m/s. A further decrease in the inlet speed from 10 to 8 m/s led to a radical change in the shape of the spectrum. Two wider smeared peaks could be observed at 8 m/s, instead of one sharp peak. In fact, the transformation of the spectrum had already begun at 10 m/s.

This may be caused by a restructuring of the hydrodynamic instability modes of the flow above the orifice, which are excited near the resonant frequency in the frequency response band. For a more detailed analysis of such behavior of the spectra, the results of sound pressure measurements were used for all conditions of inlet airflow speed in the range from 4 to 14 m/s. Figure 5 shows the sound pressure spectra measured for all flow rates.

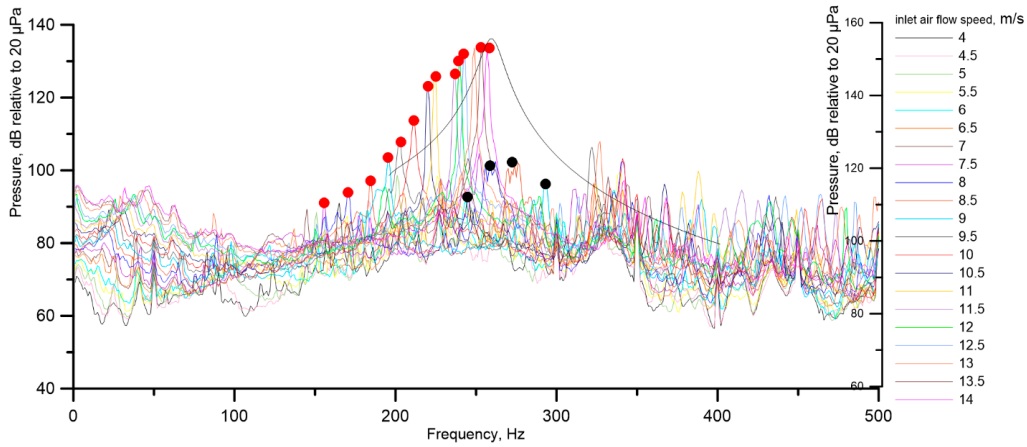

Figure 5. Sound pressure spectra for inlet airflow speed from 4 to 14 m/s with a step of 0.5 m/s. Red dots mark peaks corresponding to cases of excitation of the first mode of hydrodynamic instability. Black dots correspond to the second mode. For spectra, the vertical axis for amplitude is on the left. The solid line with the corresponding scale on the right shows the calculated frequency response of the resonator, for which the vertical axis is on the right.

The red dots indicate the positions of the top of the main peak in the spectrum, which successively decreased with decreasing flow rate, and which (as shown below) corresponded to the excitation of the first (main) hydrodynamically unstable mode. It is clearly visible that the peaks shift to the left with decreasing flow rate. On the spectrogram presented in Figure 6, this movement of the spectral peak (with a change in speed) corresponds to a highlighted (increased amplitude) line, which is close to the frequency of the peak in the frequency response characteristic of the resonator—260 Hz.

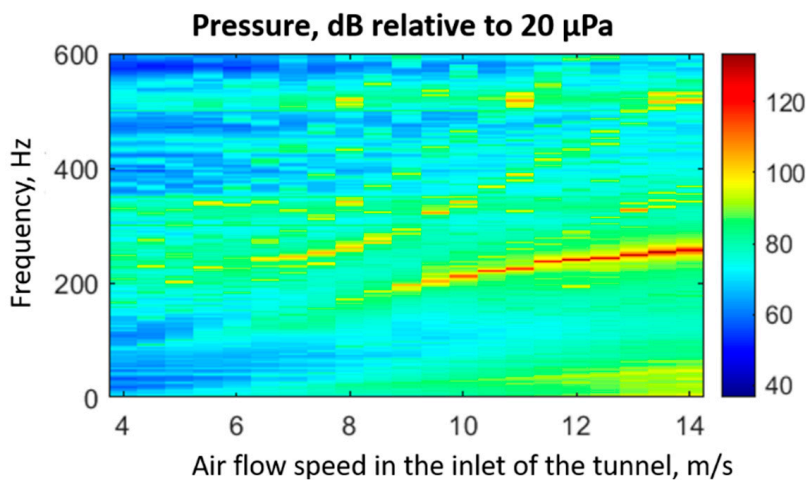

Figure 6. Spectrogram of sound pressure on the inlet air flow speed at the entrance to the working section of the wind tunnel.

One can distinguish another less-pronounced line, in which the amplitude becomes comparable to the main one only at low inlet airflow speeds. It corresponds to the peaks of the spectra, highlighted by black dots in Figure 5 in a higher frequency region.

The affiliation of a particular frequency peak f_p in the spectra to one or another hydrodynamic unstable mode of the shear flow above the orifice can be carried out on the basis of estimates of the Strouhal number $f_p L/U$, which, as follows from many studies (see [20] for example), should take discrete values. The Strouhal number based on the convective velocity U_c of the flow (the vortex advective velocity above the orifice) must be equal to 1, 2, 3... It demonstrates the fact that when self-sustained oscillations are excited by the modes of hydrodynamic instability, the period of vortex shedding from the leading edge must be a multiple of the interval of movement of the vortices from edge to edge of the orifice. In accordance with the value of the Strouhal number, modes are designated: first (main), second, third, etc. The correct measuring of the convective velocity is very difficult, so the bulk flow velocity U_b (far from the orifice where the velocity profile reaches a constant value) is usually used. A number of studies (for a review, see, for example, [20]) indicate that the ratio between convective and bulk velocities varies within 0.3–0.5 (depending on the parameters of the oncoming boundary layer, instability mode, etc.). Thus, the discrete values of Strouhal numbers of the unstable hydrodynamic modes calculated for the bulk velocity will differ from numbers for convective velocities, taking into account these coefficients. The presented calculations were performed for all flow rates, including those at which measurements with a hot-wire anemometer near the orifice were not carried out. For these, the velocity was determined using the empirical relationship between the inlet air speed and that measured velocity above the orifice (for the cases when velocity pulsations measurements were made with a hot-wire anemometer). The values of the Strouhal number plotted in Figure 7 as a function of the flow velocity above the orifice were grouped mainly around the value of 0.48 and with a slightly larger scatter of about 0.73 over the whole range of experimental conditions. These levels correspond to the excitation of the first (main) mode of hydrodynamic instability, and the second mode, respectively, in the flow above the orifice of a spherical Helmholtz resonator with given geometric dimensions.

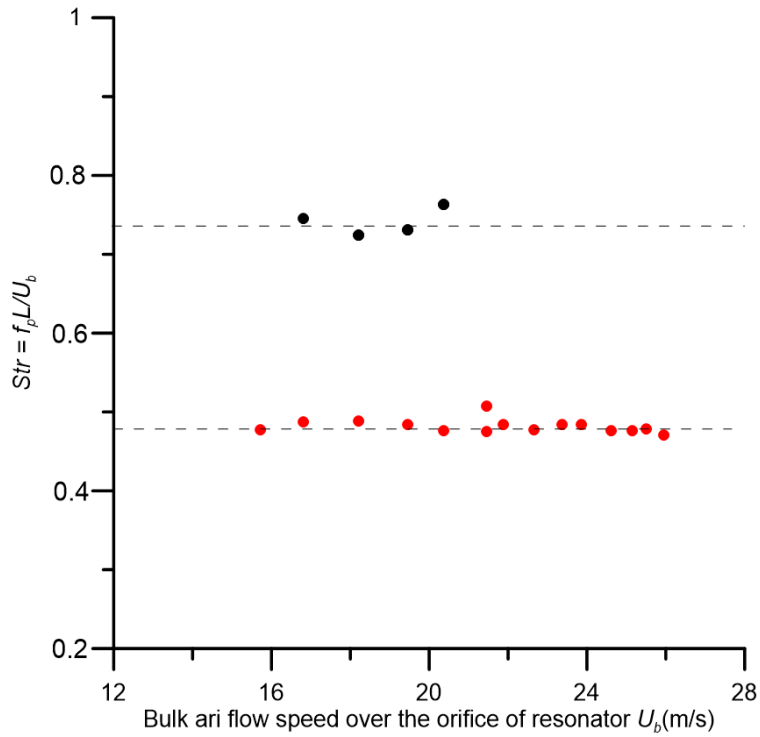

Figure 7. Dependence of the Strouhal number calculated from the peak frequency in the spectrum in Figure 5 and bulk flow velocity above the orifice. The red dots show the values for the first (main) mode of hydrodynamic instability; the black dots show the values for the second one.

Analyzing the spectra, it should also be noted that the peaks obtained in them, corresponding not only to the first but also to the second mode of hydrodynamic instability, lie in a band close to that obtained numerically. It was superimposed on the spectra in Figure 5 (taking into account the scale shift in amplitude).

3. Numerical Modeling

3.1. Calculation of the Frequency Response of the Resonator

The resonance frequency response characteristic of the spherical resonator in our work was obtained numerically by using the finite-element model within original software "SATES". The acoustic finite element model represented a spherical resonator surrounded by air volume. The walls of the resonator were modeled as a rigid body, on the outer boundary of the spherical air volume impedance elements installed, which made it possible that no reflection of the acoustic waves came back into the computational region. The excitation of the resonator was simulated by a single dipole source located at the center of the orifice and oriented along the x axis. Figure 8 shows the numerical model used by the software SATES 2.0. Red lines show impedance elements. The calculation result (earlier, in Figure 1) and the frequency response are shown together with the measurement results in Figure 5.

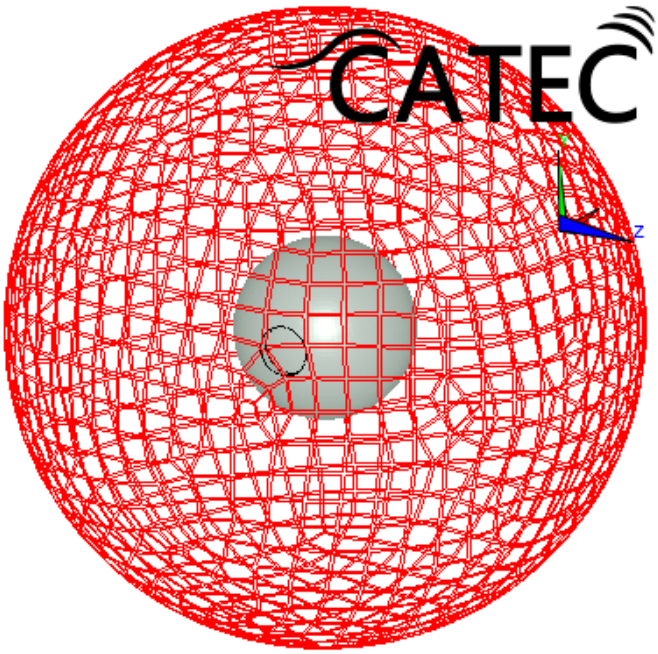

Figure 8. Illustration of numerical model of the resonator in the software SATES 2.0.

3.2. Description of Procedures of Numerical Modeling of Aeroacoustics, Calculation Results, and Comparison with Experimental Data

Calculations were performed for the air flow around a spherical resonator within the configuration, similar to the verification experiment on the wind tunnel described in the previous section. Figure 9 shows the computational domain, including the Helmholtz resonator (with geometric characteristics that fully corresponded to the laboratory experiment), placed in the working section of the wind tunnel, by analogy with the laboratory experiment. Yellow markers are control points, in which values of the three velocity components and pressure were recorded during the solution process for further processing.

The inlet airflow speed was set at the input boundary of computational domain (see the Figure 9) 1 with a turbulence intensity of 1%. This speed was equal to that in the experiment. The average pressure excess at outlet boundary 2 was assumed to be zero, and the condition of no slip was specified on the side walls of the working section 3 and the surface of the sphere 4.

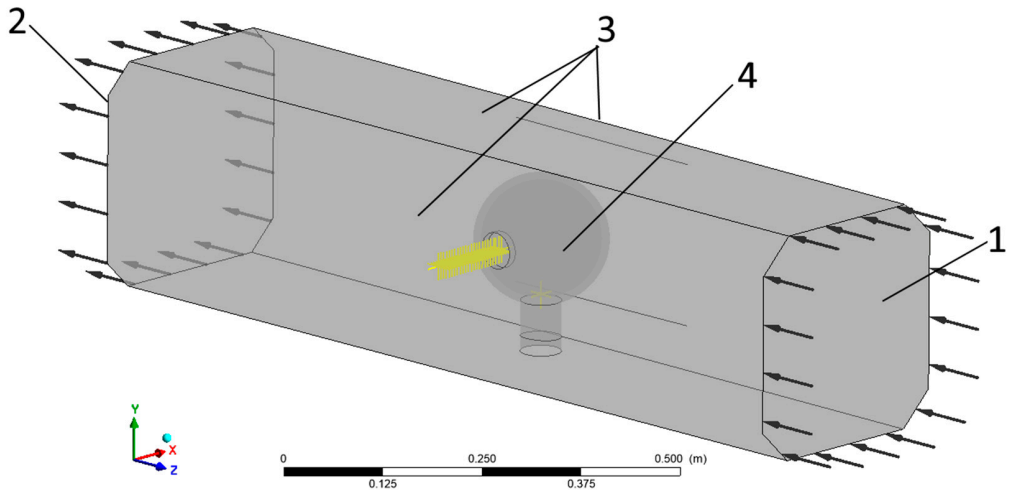

Figure 9. Computational domain of the air flow around a resonator. 1—inlet boundary, 2—outlet boundary, 3—side walls, 4—surface of the sphere.

The solution of the problem In the first formulation was carried out using the simplest turbulence model from the URANS class. In the context of this turbulence model, the averaged Navier–Stokes equations for a compressible ideal gas are solved and described by the following equations (while the time averaging signs are omitted for brevity):

$$\begin{cases} \frac{\partial \rho}{\partial t} + \frac{\partial(\rho u_k)}{\partial x_k} = 0, \\ \frac{\partial(\rho u_i)}{\partial t} + \frac{\partial(\rho u_i u_k)}{\partial x_k} = -\frac{\partial \overline{p}}{\partial x_i} + \frac{\partial\left(\tau_{ik}+\tau_{t,ik}\right)}{\partial x_k}, \\ \frac{\partial(\rho E)}{\partial t} + \frac{\partial(\rho u_k H)}{\partial x_k} = \frac{\partial}{\partial x_k}[u_i(\tau_{ik} + \tau_{t,ik}) - (q_k + q_{t,k})], \\ \rho = \frac{pm}{(RT)} \end{cases} \tag{2}$$

Here, x_k are the Cartesian coordinates (k = 1, 2, 3); u_i are the components of the velocity vector of the averaged flow; E and H are the specific total energy and total enthalpy of the gas; T is the temperature; R is the universal gas constant; and m is the molecular mass. The components of the molecular viscous stress tensor τ_{ik} and the heat flux density vector due to the molecular thermal conductivity q_k are determined, respectively, using Newton's rheological law and Fourier's law. The components of the Reynolds stress tensor $\tau_{t,ik}$ and the Reynolds heat flux vector $q_{t,k}$ are determined using Mentor's Shear Stress Transport (SST) turbulence model.

The two-parameter turbulence model SST has the following formulation:

$$\begin{cases} \frac{\partial(\rho k)}{\partial t} + \frac{\partial(\rho k u_k)}{\partial x_k} = \frac{\partial}{\partial x_k}\left((\mu + \sigma_k \mu_t)\frac{\partial k}{\partial x_k}\right) + P_k - \rho\beta^* k\omega, \\ \frac{\partial(\rho\omega)}{\partial t} + \frac{\partial(\rho\omega u_k)}{\partial x_k} = \frac{\partial}{\partial x_k}\left((\mu + \sigma_k \mu_t)\frac{\partial \omega}{\partial x_k}\right) + (1 - F_1)\frac{2\rho\sigma_{\omega 2}}{\omega}\frac{\partial k}{\partial x_k}\frac{\partial \omega}{\partial x_k} + \gamma\frac{\rho}{\mu_t}P_k - \rho\beta_3\omega^2, \end{cases} \tag{3}$$

where F_1 function is a switch between k-ω and k-ε turbulence models.

This model of turbulence was used due to the assumption that it is necessary to determine the narrowband component of the frequency spectrum of velocity pulsations. This peak corresponds to the frequency of vortex shedding from the leading edge of the orifice, which is synchronized with the resonance frequency of the resonator volume.

This approach demands relatively small requirements (in comparison with the scale resolving simulation approach) for the computational grid model, i.e., to resource greediness. The Menter's SST turbulence model (SST) was used to close the system of Reynolds-averaged Navier–Stokes equations.

A block-structured grid model in the computational domain divided into cells consisting of hexahedral elements was used. Figure 10 shows a general view of the grid model

GM1 (1.2 million cells) with selected fragments near the resonator, developed to formulate the problem using the SST turbulence model.

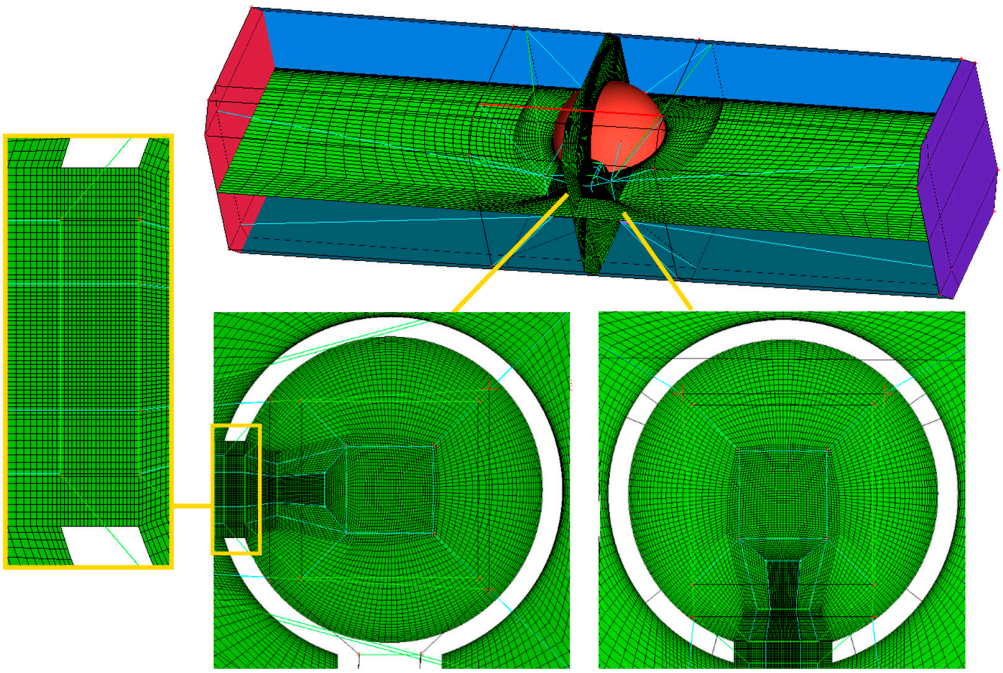

Figure 10. Grid model (GM1) of the computational domain with selected fragments for the SST turbulence model.

Fields of hydrodynamic characteristics (velocity, vorticity, pressure) were obtained inside the computational domain determined on the grid model GM1. The vorticity field at the cross-section plane of symmetry of the resonator at the inlet airflow speed of 14 m/s is shown in Figure 11. It was possible to simulate the process of shedding of a vortex from the leading edge of the orifice and its transfer to the trailing edge by analogy with the works [10,20].

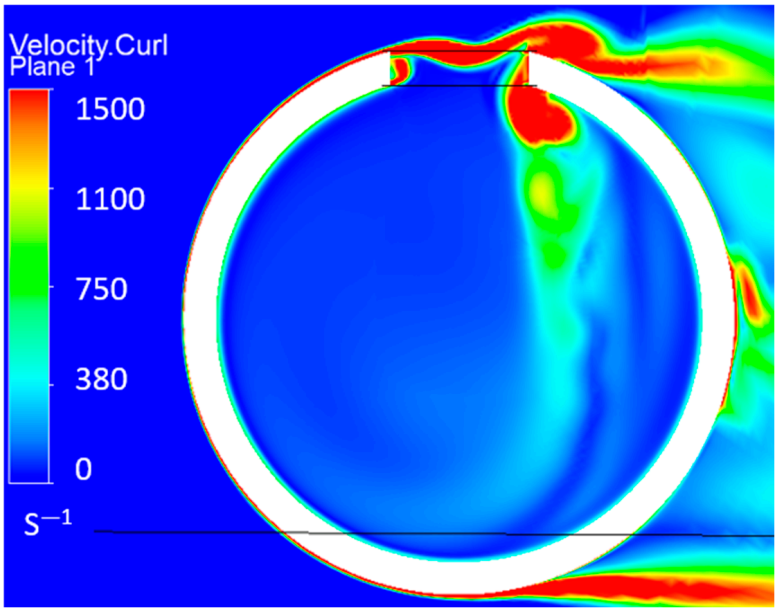

Figure 11. The calculated vorticity field at the cross-sectional plane of symmetry of the resonator, inlet air flow 14 m/s. URANS.

A comparison of the calculated pressure pulsation power spectra in the center of the resonator for four different flow rates (8, 10, 12, 14 m/s) for the SST model (dashed lines) with those measured experimentally in the wind tunnel (solid lines) is shown in Figure 12.

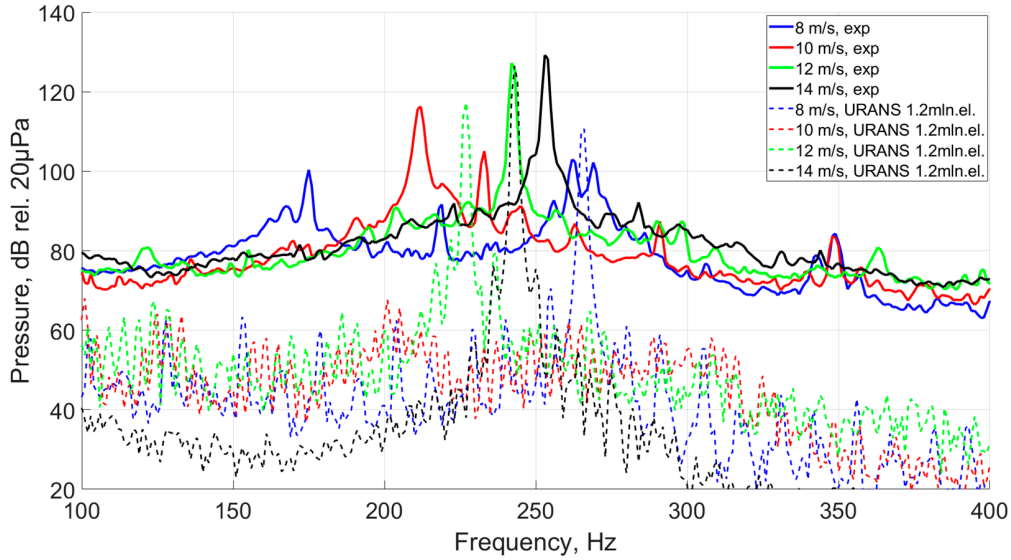

Figure 12. The sound pressure pulsation spectra for different flow rates (experimental data and results of calculations).

Narrowband peaks in the spectrum corresponding to the frequencies of vortex shedding from the leading edge were well distinguished. At speeds of 12 and 14 m/s, the discrepancy between the calculation and experiment frequency for peaks was about 4–6%, and in pressure level 3–10 dB. The data are inconsistent at the 10 m/s transient regime due to the specific property of the SST turbulence model. The feature is concerned with setting the averaging period of hydrodynamic fields relative to energy-transfer vortices using the model. Here, this period is determined by the frequency of the dominated non-stationary process in the system, and since the mode of instability changes from the first to the second with approximately the same order of magnitude, there is an uncertainty in the choice of the averaging period (frequency of dominating energy-transfer vortices) at a speed of 8–10 m/s. It should be noted that the SST turbulence model does not reproduce background turbulence, and therefore the characteristics studied outside the resonant frequency cannot fundamentally coincide with experiment.

To compare with the results of SST modeling, another numerical model was used for calculations in the scale-resolving simulation (SRS) using the WMLES (Wall-Modeled Large Eddy Simulation) model based on the same SST model. The mathematical formulation of this approach differs from RANS only in the description of additional terms in the right part of the equations of motion and energy. Instead of the components of the Reynolds stress tensor $\tau_{t,ik}$ and the Reynolds heat flux vector $q_{t,k}$ (see the Formula (2), there are spatially filtered (but unlike the RANS formulation, there are instantaneous values of the terms here) nonlinear convective terms of the Navier–Stokes equations $\tau_{sgs,ik}$ and $q_{sgs,k}$, where the sgs indices indicate a sub-grid scale.

In the context of this turbulence model, all the disturbances with scales that were larger than several cells of the grid model were directly resolved, and the energy of unresolved turbulence of smaller scales was compensated by sub-grid viscosity. In this case, the boundary layer was divided into two parts because of the requirement for the fineness of the grid model due to the significant decrease in the scale of energy-transfer vortices as we became closer to the streamlined wall in the boundary layer. The SRS model operates in the outer region (as in the free flow), and near the wall the SST model is activated, which compensates for the unresolved part of the boundary layer energy.

To formulate the problem using the WMLES turbulence model, the sizes of the grid elements were reduced by half compared to SST. Thus, the grid model GM2 was formed (see Figure 13). The total number of elements in GM2 was almost 10 million.

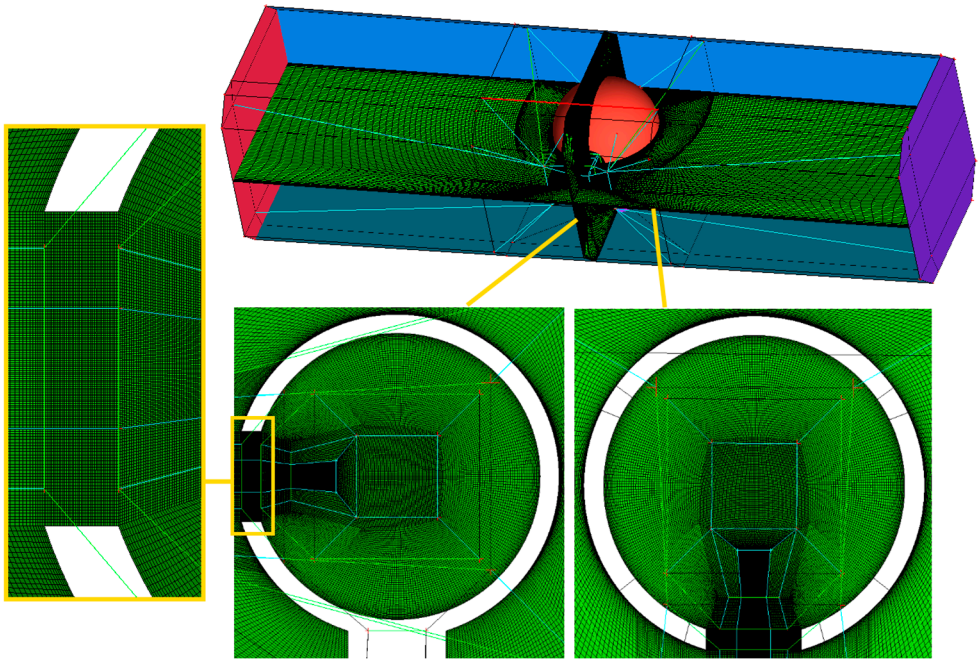

Figure 13. Grid model (GM2) of the computational domain with selected fragments for the WMLES turbulence model.

An example of the obtained vorticity field using the WMLES model at the cross-section plane of symmetry of the resonator at the inlet airflow speed of 14 m/s is showed on Figure 14. Comparing Figures 11 and 14, it is clear that the vortex structure formed at the leading edge of the resonator orifice, breaking up on the lower edge, fragments up into smaller vortex structures and their intensity is greater, compared to the results with the URANS formulation.

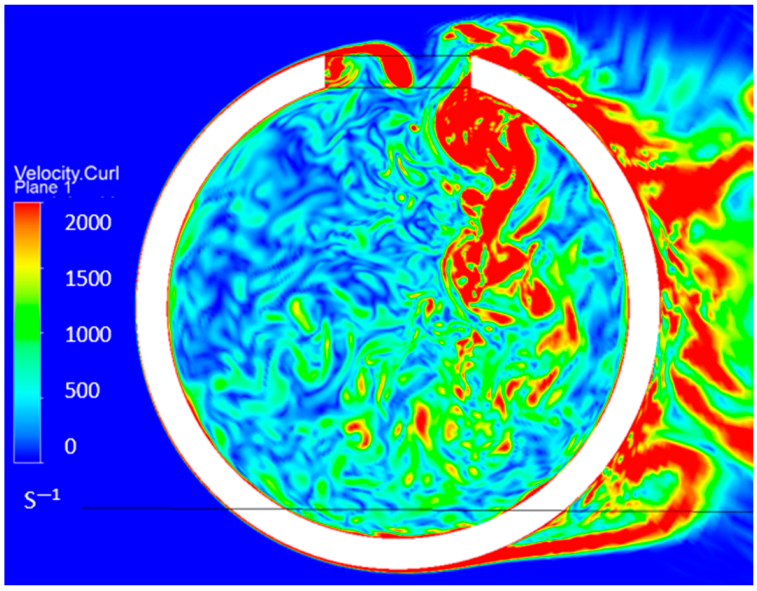

Figure 14. The calculated vorticity field at the cross-sectional plane of symmetry of the resonator, inlet air flow 14 m/s. WMLES.

The pressure pulsation spectra obtained in the SRS formulation (dashed lines) are presented together with the previous results for the URANS formulation in Figure 15 for similar flow conditions. There is a good agreement between the levels and frequencies of resonances for velocities of 10, 12 and 14 m/s with experimental data. Moreover, the calculations better reproduce the background level of pulsations, in contrast to the SST turbulence model. The spectral peaks of the resonances, due to the short total time realization, have a larger width than in the experiment, which can be eliminated by the accumulation of a longer time realization during the calculation process in further investigations. For the transition regime at an inlet speed of 8 m/s, where a rivalry between the first and second modes of hydrodynamic instability occurred, the discrepancy with the experiment is significant (25% in frequency and 10 dB in level) for the first mode. For the second mode at this speed, the frequency error is only 2% if we consider it relative to the middle of the wide peak obtained from the experimental results.

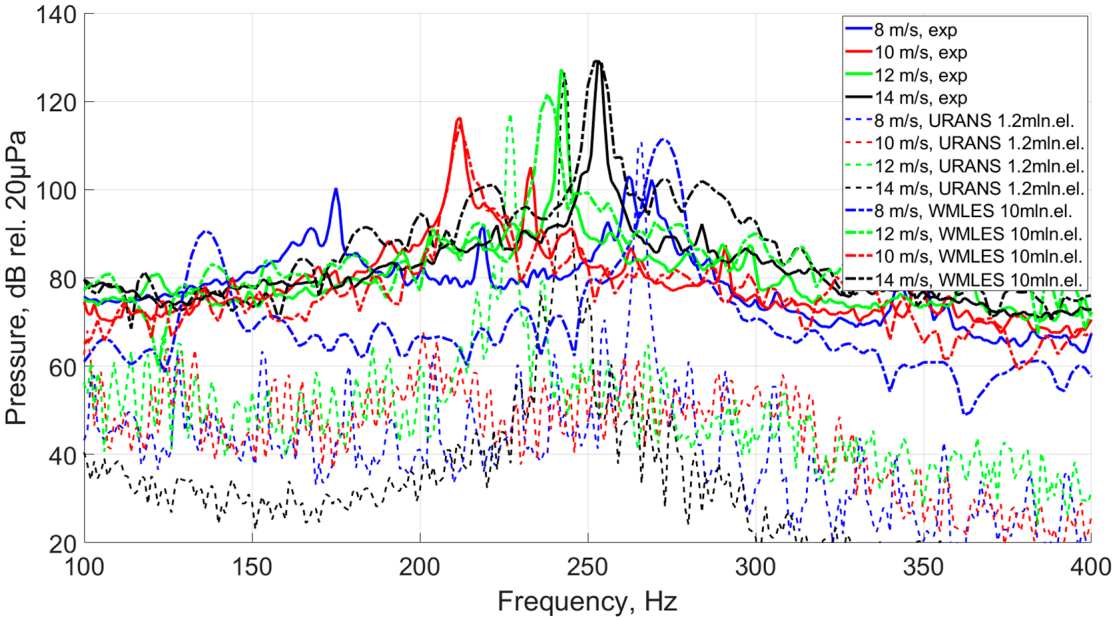

Figure 15. The sound pressure pulsation spectra for different flow rates (experimental and calculated data: SST, WMLES).

The influence of grid model parameters on the resulting hydrodynamic characteristics for the SST and WMLES turbulence models has different behavior. A refinement of the grid model in the case of the SST model (mainly in the unsteady flow region) leads to convergence on the "model" solution, determined by the settings of the turbulence model. In the WMLES model, the refinement of the grid model brings us closer to the direct solution of the Navier–Stokes equations, which describe the physical process "as it is", in contrast to the previous one. To clarify the effect of refinement of the grid model on the hydrodynamic characteristics for this problem, the SST and WMLES turbulence models were used with both of the GM2 and GM1 grid models, respectively.

The SST turbulence model on the finer grid model GM2 allowed one to determine the pressure inside the resonator more accurately, as is shown in Figure 16. This indicates the correct settings of the turbulence model for this class of problems (constants set by the default in software). Moreover, in terms of accuracy, they are completely close to the results obtained in the SRS formulation with the same grid model. The results of solving the problem using the WMLES turbulence model in combination with the less-fine grid model GM2 gave some unexpected results (from the first point of view). An increase in the size of the elements led to not only a decreasing amplitude of pulsations at the resonance frequency, which looked true because less energy can be resolved directly in this case, but also to a shifting of the resonance frequency. This effect may be associated with the

evaluation of the boundary layer in the region above the orifice, where the flow becomes unstable. To confirm this assumption, additional research with a finer grid in the boundary layer in the area of the orifice with the same grid parameters outside the boundary layer is needed.

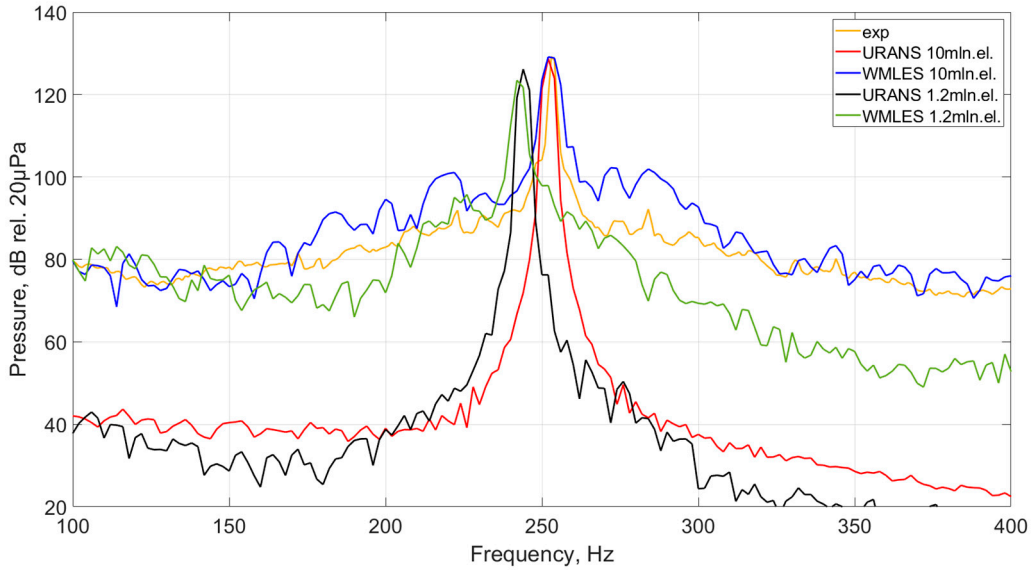

Figure 16. The sound pressure pulsation spectra for air flow 14 m/s (experimental and calculated data: SST, WMLES).

From the point of view of resource greediness, expressed in the number of core hours spent on obtaining a solution, both turbulence models turned out to be almost equivalent when using the same grid models. This is most likely due to the implementation of numerical schemes, as well as turbulence models in specific software.

Table 1 summarized the data on the resources spent in solving this problem, expressed in processor time—the number of cores involved in solving multiplied by the time (in hours) of the solver for all arrangements of numerical modeling. The characteristics of a high-performance computer system are two processors with 20 Intel(R) Xeon(R) Gold 6230 cores at a frequency of 2.10 GHz.

Table 1. Processor time for all arrangements of numerical modeling.

Model, Number of Cells	WMLES, 10 mln	URANS, 10 mln	WMLES, 1.2 mln	URANS, 1.2 mln
Core × hours	18,084	16,595	914	755

The advantage of the WMLES turbulence model compared to SST (from the point of view of the determined frequency response) is concerned with the correct estimation of background turbulence outside the narrowband resonance. This can be useful in studies where, in addition to the well-pronounced resonance frequency due to the effects of compressibility of the media inside the resonator, the system also contains structural resonances at which, under the influence of a broadband source, the level of acoustic radiation can also locally increase.

4. Conclusions

We carried out studies on various computational fluid dynamics approaches applied to the description of self-sustained oscillation in the free-flow-excited Helmholtz resonator system. During a special benchmark laboratory experiment in the wind tunnel of the Institute of Applied Physics RAS, it was possible to obtain various regimes, both of self-sustained oscillations, with one clearly distinguished mode of hydrodynamic instability, and transient modes with modes concurrence. The obtained experimental data were used

to verify the results of the calculation released within the framework of two fundamentally different approaches to turbulence modeling: URANS modeling and SRS modeling (in the WMLES implementation). The calculation results showed that the URANS approach (with the closure of the SST turbulence model) gives a good result for predicting the frequency response at resonance on a coarse grid model, and an excellent result on a fine grid model. At the same time, the SRS approach (specifically the WMLES model) gives similar results on the same grid models; however, in addition to the resonant frequency, it also predicts the broadband component of the acoustic spectral characteristics. In addition, it is noteworthy that the time spent obtaining a solution is almost the same for both approaches, and depends only on the fineness of the grid model used.

Author Contributions: Conceptualization, D.S. and K.P.; measurements, A.S. and D.S.; numerical modeling, V.E. and I.V.; validation, D.S. and I.V. All authors have read and agreed to the published version of the manuscript.

Funding: This research was funded by the state task of the Institute of Applied Physics of Russian Academy of Sciences; the theme is "Creation of key elements of supercomputer acoustic design technology" (FFUF-2022-0003).

Data Availability Statement: The data presented in this study are available in the article.

Conflicts of Interest: Author Kirill Pyalov was employed by the company CDB ME Rubin. The remaining authors declare that the research was conducted in the absence of any commercial or financial relationships that could be construed as a potential conflict of interest.

References

1. Kinsler, L.E.; Frey, A.R.; Coppens, A.B.; Sanders, J.V. *Fundamentals of Acoustics*, 4th ed.; John Wiley and Sons Inc.: Hoboken, NJ, USA, 2000; pp. 1–550.
2. Gautam, A.; Celik, A.; Azarpeyvand, M. An Experimental and Numerical Study on the Effect of Spacing between Two Helmholtz Resonators. *Acoustics* **2021**, *3*, 97–117. [CrossRef]
3. Thomas, R.H.; Burley, C.L.; Olson, E.D. Hybrid wing body aircraft system noise assessment with propulsion airframe aeroacoustic experiments. *Int. J. Aeroacoust.* **2012**, *11*, 369–409. [CrossRef]
4. Groby, J.-P.; Lagarrigue, C.; Brouard, B.; Dazel, O.; Tournat, V.; Nennig, B. Enhancing the Absorption Properties of Acoustic Porous Plates by Periodically Embedding Helmholtz Resonators. *J. Acoust. Soc. Am.* **2015**, *137*, 273–280. [CrossRef] [PubMed]
5. Dogra, S.; Gupta, A. Design, Manufacturing, and Acoustical Analysis of a Helmholtz Resonator-Based Metamaterial Plate. *Acoustics* **2021**, *3*, 630–641. [CrossRef]
6. Howe, M.S. *Acoustics of Fluid-Structure Interactions*; Cambridge University Press: New York, NY, USA, 1998; pp. 1–560.
7. Chaterllier, L.; Laumonier, J.; Gervais, Y. Theoretical and experimental investigations of low Mach number turbulent cavity flows. *Exp. Fluids* **2004**, *36*, 728–740. [CrossRef]
8. Panton, R.L.; Miller, J.M. Excitation of a Helmholtz resonator by turbulent boundary layer. *J. Acoust. Soc. Am.* **1975**, *58*, 800–806. [CrossRef]
9. Elder, S.A.; Farabee, T.M.; DeMetz, F.C. Mechanisms of flow-excited cavity tones at low Mach number. *J. Acoust. Soc. Am.* **1982**, *72*, 532–549. [CrossRef]
10. Nelson, P.A.; Halliwell, N.A.; Doak, P.E. Fluid dynamics of a flow excited resonance. Part I: Experiment. *J. Sound Vib.* **1981**, *78*, 15–38. [CrossRef]
11. Nelson, P.A.; Halliwell, N.A.; Doak, P.E. Fluid dynamics of a flow excited resonance. Part II: Flow acoustic interaction. *J. Sound Vib.* **1983**, *91*, 375–402. [CrossRef]
12. Panton, R.L. Effect of orifice geometry on Helmholtz resonator excitation by grazing flow. *AIAA J.* **1990**, *28*, 60–65. [CrossRef]
13. Amandolese, X.; Hemon, P.; Regardin, C. An experimental study of the acoustic oscillations by flows over cavities. *J. Vib. Acoust.* **2004**, *126*, 190–195. [CrossRef]
14. Dequand, S.; Luo, X.; Willems, J.; Hirschberg, A. Helmholtz-like resonator self-sustained oscillations. Part 1: Acoustical measurements and analytical models. *AIAA J.* **2003**, *41*, 408–415. [CrossRef]
15. Dequand, S.; Hulshoff, S.; van Kuijk, H.; Willems, J.; Hirschberg, A. Helmholtz-like resonator self-sustained oscillations. Part 2: Detailed flow measurements and numerical simulations. *AIAA J.* **2003**, *41*, 416–423. [CrossRef]
16. Elder, S.A. Self-excited depth-mode resonance for a wall-mounted cavity in turbulent flow. *J. Acoust. Soc. Am.* **1978**, *64*, 877–890. [CrossRef]
17. Mast, T.D.; Pierce, A.D. Describing-function theory for flow excited resonators. *J. Acoust. Soc. Am.* **1995**, *97*, 163–172. [CrossRef]
18. Kook, H.; Mongeau, L. Analysis of the periodic pressure fluctuations induced by flow over a cavity. *J. Sound Vib.* **2002**, *251*, 823–846. [CrossRef]

19. Komkin, A.; Bykov, A.; Saulkina, O. Evaluation of the Oscillation Velocity in the Neck of the Helmholtz Resonator in Nonlinear Regimes. *Acoustics* **2022**, *4*, 564–573. [CrossRef]
20. Ma, R.; Slaboch, P.E.; Morris, S.C. Fluid mechanics of the flow-excited Helmholtz resonator. *J. Fluid. Mech.* **2009**, *623*, 1–26. [CrossRef]
21. Sergeev, D.A. A measuring system for studying liquid flows by the particle image velocimetry method based on a diode-pumped solid-state laser. *Instrum. Exp. Tech.* **2009**, *52*, 438–444. [CrossRef]
22. Crouse, B.; Senthooran, S.; Freed, D.; Balasubramanian, G.; Gleason, M.; Puskarz, M.; Lew, P.; Mongeau, L. Experimental and numerical investigation of a flow-induced cavity resonance with application to automobile buffeting. In Proceedings of the 12th AIAA/CEAS Aeroacoustics Conference, Cambridge, MA, USA, 8–10 May 2006.
23. Sevryukov, O.F.; Sokov, E.M.; Suvorov, A.S.; Salin, M.B.; V'yushkina, I.A.; Eremeev, V.O.; Smirnov, S.A.; Evstifeev, V.V.; Lvova, D.A.; Myakishev, I.V.; et al. Certificate for a Computer Program. 2022663702 Russian Federation "SATES-DK" (SATES 2.0); IAP RAS—No. 2022662548, publ. 19 July 2022.

Disclaimer/Publisher's Note: The statements, opinions and data contained in all publications are solely those of the individual author(s) and contributor(s) and not of MDPI and/or the editor(s). MDPI and/or the editor(s) disclaim responsibility for any injury to people or property resulting from any ideas, methods, instructions or products referred to in the content.